

Quantitative Computed Tomography Analysis of Local Chemotherapy in Liver Tissue After Radiofrequency Ablation¹

Agata A. Exner, PhD, Brent D. Weinberg, BS, Nicholas T. Stowe, PhD, Anthony Gallacher, MS, David L. Wilson, PhD, John R. Haaga, MD, Jinming Gao, PhD

Rationale and Objectives. Computed tomography (CT) was used to noninvasively monitor local drug pharmacokinetics from polymer implants in rat livers before and following radiofrequency ablation.

Materials and Methods. Polymer matrixes containing carboplatin (a platinum-containing chemotherapeutic agent) were implanted into rat livers either immediately after radiofrequency ablation ($n = 15$) or without prior treatment ($n = 15$). The animals were divided into five subgroups ($n = 3$ per group) and subjected to a terminal CT scan at 6, 24, 48, 96, or 144 hours. Carboplatin concentration in tissue and within the implant matrix was correlated with CT intensity, and standard curves were produced for each environment. This correlation was used to evaluate the differences in drug transport properties between normal and ablated rat livers. A quantitative image analysis method was developed and used to evaluate the release rate and tissue distribution of carboplatin in normal and ablated liver tissue. The CT data were validated by previously reported atomic absorption spectroscopy measurement of implant and tissue drug levels.

Results. Correlation of carboplatin concentration and Hounsfield units results in a linear relationship with correlation coefficients (slopes) of 15 and 4 Hounsfield units/(mg/mL), for carboplatin in tissue and polymer, respectively. Noninvasive monitoring of local pharmacokinetics in normal and ablated tissues indicates that ablation before local carboplatin delivery increases the retention of carboplatin within the polymer matrix and drastically increases the drug retention in the ablated tissue volume (over 3-fold difference) resulting in a higher average dose to the surrounding tissue. At 1.6 mm from the implant boundary, carboplatin concentration is significantly higher in ablated tissue at 48, 96, and 144 hours ($P < .05$), and reaches 4.7 mg/mL in ablated tissue at 48 hours. In comparison, the concentration in normal liver at 1.6 mm reaches only 0.7 mg/mL at the same time point. The drug penetrates 3.1 mm in ablated liver compared with 2.3 mm in normal liver also at 48 hours. After 144 hours, the drug is still detected at 3.1 mm in ablated liver but not in normal liver. The differences are significant ($P < .05$) at both 48 and 144 hours. Correlation with chemical analysis suggests that CT data accurately predicts the drug pharmacokinetics in both ablated and normal livers.

Conclusion. This work shows that X-ray CT imaging is a useful and promising technique for in vivo monitoring of the release kinetics of locally delivered radiopaque agents.

Key Words. Noninvasive pharmacokinetic imaging; controlled release drug delivery; radiofrequency ablation; computed tomography.

© AUR, 2004

Acad Radiol 2004; 11:1326–1336

¹ From the Department of Radiology, Case Western Reserve University School of Medicine, Cleveland, OH (A.A.E., J.R.H., J.G.); the Department of Biomedical Engineering, Case Western Reserve University, Cleveland, OH (B.D.W., D.L.W., J.G.); the Department of Surgery, Case Western Reserve University School of Medicine, Cleveland, OH (N.T.S.); and the Department of Analytical Chemistry, Ricerca Biosciences, LLC, Concord, OH (A.G.). Received January 5, 2004; revision requested March 24; received April 27; accepted September 28. Supported by the National Institutes of Health grant nos. R21 CA093993 and R01 CA90696 (to J.G.). **Address correspondence to** A.A.E. Department of Radiology, University Hospitals of Cleveland, 11100 Euclid Ave, Bishop s609, Cleveland, OH 44106-5056; e-mail: exner@uhrad.com

© AUR, 2004

doi:10.1016/j.acra.2004.09.007

Site-specific drug delivery is a desirable scheme that aims to elevate the drug concentration directly at the target site while limiting systemic effects of toxic drugs; intratumoral drug delivery is one example of this approach. Although an outwardly simple concept, the development of site-specific delivery systems has been hampered because of the lack of accurate local pharmacokinetic analysis techniques. Because conventional analysis of drug concentration in plasma and urine does not directly reflect drug concentration at the site of action, a more direct visualization and analysis method is desirable to accurately characterize the *in vivo* properties of any such device.

Because it addresses this and many other needs, noninvasive pharmacokinetic imaging is quickly becoming a vital tool to facilitate the development of new drugs and drug delivery methods. Diagnostic imaging techniques such as positron emission tomography, single photon emission computed tomography, and magnetic resonance imaging have been used extensively to study drug distribution and metabolism in patients with various types of cancer (1–5). However, limitations such as low spatial resolution, radioactive half-life restrictions, long image acquisition time, and the need for radiopharmaceutical production restrict their applications in pharmacokinetic monitoring (2,3).

In this study, we used clinical X-ray computed tomography (CT) as an imaging modality for tracking the characteristic behavior of an interstitial drug delivery device *in vivo*. Compared with other noninvasive imaging techniques, CT provides outstanding spatial resolution and speed without need for radiolabeling the drugs and risking alteration of transport properties. Furthermore, when compared with traditional pharmacokinetic studies, which gather needed data from the collection of blood or tissue samples, CT monitoring presents a localized and noninvasive alternative.

Noninvasive pharmacokinetic monitoring is particularly important in cases where *in vitro* (or test tube) dissolution characterization of a drug delivery device does not correspond well to the *in vivo* system, such as in the case of tumor tissue after radiofrequency ablation treatment, where the physiologic parameters have been severely altered from the baseline of healthy tissue. A number of studies have shown that the vasculature of the ablated tissue is completely destroyed, leading to a low-perfusion environment that can have a significant impact on drug delivery to the area (6–10). Because one of the initiatives of our laboratory is the development of a local chemotherapy that can be used in conjunction with radiofre-

quency ablation to control any local tumor recurrence after this treatment, the data gathered with this pharmacokinetic imaging technique will be invaluable in the future development of this device.

The combination of CT imaging and quantitative image analysis can potentially provide a direct method for the evaluation of the transport of drugs released from a localized, controlled release device *in vivo*. We hypothesize that noninvasive monitoring of local drug delivery using CT will lead to the successful assessment of drug pharmacokinetics that cannot be normally observed with *in vitro* or *ex vivo* analysis. The results obtained here should serve as a validation of the CT technique for future applications and should improve our understanding of the damage inflicted on tissue by the radiofrequency ablation treatment and its implications in localized chemotherapy.

MATERIALS AND METHODS

The present study attempts to use CT imaging to noninvasively characterize and differentiate pharmacokinetics of a local drug delivery system in normal and ablated liver tissue. All animal procedures followed a protocol approved by the Institutional Animal Care and Use Committee. Experiments consisted of: (1.) treatment of rat livers with radiofrequency ablation and/or insertion of biodegradable carboplatin implant; (2.) monitoring of local carboplatin release and tissue distribution over 144 hours with CT; (3.) development and application of quantitative CT image analysis to describe the local pharmacokinetics of carboplatin in tissue; and (4.) correlation of the CT data with atomic absorption analysis of the same system.

Experimental Groups

Thirty male Sprague Dawley rats (250–350 g, Charles River Laboratories, Wilmington, MA) were used for this study. The animals were divided into two treatment groups, those undergoing radiofrequency ablation followed by site-specific placement of carboplatin implants ($n = 15$) and those receiving carboplatin implants with no additional treatment ($n = 15$). Within each treatment group, the animals were assigned to five subgroups ($n = 3$) with endpoints at 6, 24, 48, 96, or 144 hours after treatment.

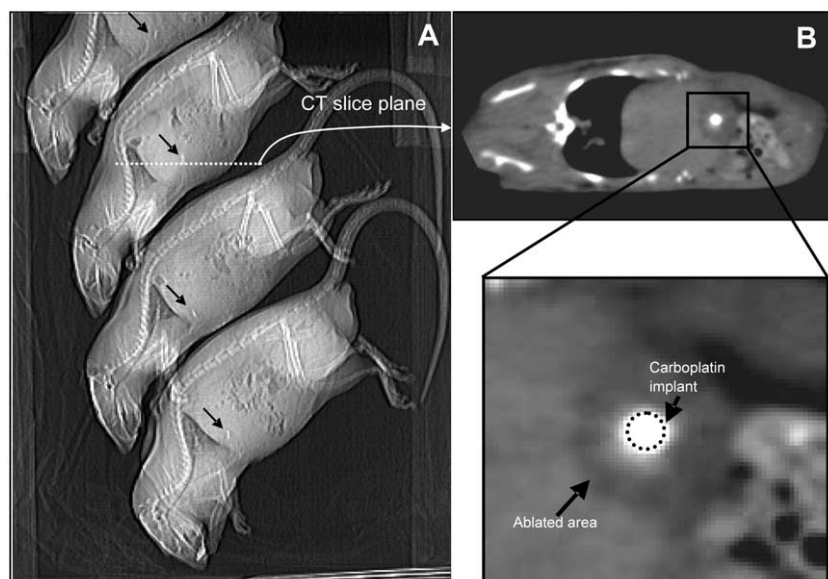


Figure 1. Representative images acquired with x-ray CT. **(a)** Planar scout CT showing orientation of rats and the axial scan plane perpendicular to the millirod axis (arrows). **(b)** Typical CT "slice" showing a cross-section of carboplatin millirod implanted in an ablated liver. The inset shows an enlarged image of the area immediately adjacent to the implant.

Carboplatin Implant Fabrication

PLGA (Birmingham Polymers, Inc, Birmingham, AL) implants containing carboplatin (Sigma-Aldrich, Milwaukee, WI) were fabricated according to a previously established compression-heat molding procedure (11). Briefly, PLGA microspheres were mixed with carboplatin powder to form a uniform mixture, and D(+)-glucose was added to the mixtures to expedite the rate of release. The homogeneously mixed powder was placed in a mold and compressed at 4.6×10^6 Pa and 90°C for 2 hours. The cylindrical implants had an average diameter of 1.6 mm and a loading density of 10% carboplatin (average expected dose of $8 \mu\text{g/g}$ body mass, based on 300 g rat).

Radiofrequency Ablation and Implantation of Carboplatin Delivery Devices

Rats were anesthetized using an intraperitoneal injection of sodium pentobarbital and the liver was exposed through a midline incision. In animals undergoing ablation ($n = 15$), the liver tissue was ablated at $90 \pm 3^\circ\text{C}$ for 2 minutes with a 19-gauge radiofrequency ablation needle electrode (Radionics, Burlington, MA). After ablation, carboplatin implants (5–7 mm in length) were implanted into the center of ablated tissue and the abdomen was closed. In rats receiving only carboplatin implants ($n = 15$), the abdomen was opened, and the exposed liver

was perforated with an 18-gauge hypodermic needle. Implants of the same composition were then placed into the liver parenchyma, and the abdomen was closed. All animals received buprenorphine following the surgery and were allowed to recover.

CT Imaging of Local Drug Release

To monitor the release of drug from each of the implanted millirods, anesthetized rats were imaged with a helical CT system (Mx8000, Philips Medical Systems, Andover, MA). Each rat was positioned in the scanner so that the image plane was approximately perpendicular to the long axis of the millirod. Figure 1 shows a typical image acquisition scheme. The planar CT scout image shows the orientation of the rats with respect to the scan plane (Fig. 1A). Figure 1B shows an example CT slice through an ablated liver (6 days after implantation). The same position was maintained throughout the study and recreated as closely as possible at the different imaging sessions. CT scans had the following settings: helical scan, 120 kVp, 480 mAs, 0.5 pitch, and 0.8 mm effective slice thickness. Rats were scanned at 6, 24, 48, 96, and 144 hours following implantation and were euthanized with an overdose of sodium pentobarbital immediately following the scan.

Evaluation of Drug Pharmacokinetics

The CT data underwent extensive processing to evaluate the local pharmacokinetics of carboplatin in the normal and ablated liver tissue. First, a standard curve detailing the linear relationship between Hounsfield units (HU) and carboplatin concentration was created from phantom studies. Next, an analysis regimen was developed to isolate tissue and implant levels of carboplatin from the other components in each image volume. The method begins with background subtraction of tissue and polymer attenuation, followed by circumferential averaging of the data about each cylindrical implant. Next, an inherent blur correction is applied and the analysis is concluded with a separate regional distribution analyses in the implant and tissue volumes. A detailed description of this analysis is provided below.

Correlation of HU to drug concentration.—Gelatin phantoms were used in the calculation of the conversion factor from HU to carboplatin concentration (mg/mL). Because of the small size (high spatial frequency) of the implants (1.6 mm diameter) compared with the surrounding liver tissue, two separate studies were carried out, one to determine the conversion factor for Pt contained within the millirod body and one in liver tissue. For the first study, implants of identical composition to those used in the animals were inserted into 10% (w/v) gelatin phantoms formed in 50 mL Falcon centrifuge tubes, and the drug was allowed to diffuse out for different lengths of time ranging from 1 hour to 6 days. For the latter, gelatin (also 10% w/v) was dissolved in water containing known concentrations of carboplatin (0, 0.125, 0.25, 0.5, 1.25, 2.5, 5, 7.5, and 10 mg/mL). The solutions were cooled in a 12-well polystyrene tissue culture plate for imaging and analysis. Both sets of gels were then scanned using the same CT protocol as in vivo studies (120 kVp, 480 mAs, 0.8 mm slice thickness). Following the scan, the implants were removed and the remaining drug was extracted into solution. These samples were analyzed with atomic absorption spectroscopy to determine the total amount of drug remaining in each implant (12). Average HU values were calculated within a circular region of interest for each implant and tissue phantom. This analysis was performed with ImageJ (Research Services Branch, National Institute of Mental Health, Bethesda, MD). Average HU values were plotted against carboplatin concentration to obtain the standard curves.

Sampling of CT volumes.—We used a 3-dimensional (3D) sampling method to spatially examine drug distributions

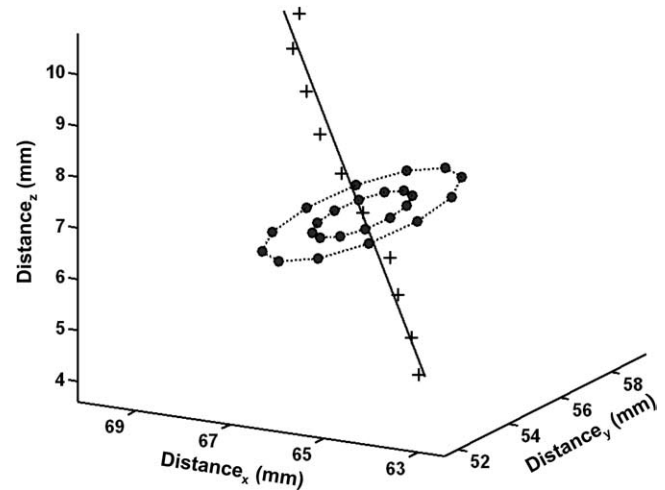


Figure 2. Representation of the algorithm used to sample the CT image volume. Centers of millirods were manually chosen on each slice (+). A least squares algorithm was utilized to fit a line through these points and image data were sampled along circles normal to the fitted line using trilinear interpolation (●).

at an orientation exactly perpendicular to the long axis of the cylindrical polymer implant. First, we manually localized the center of the millirod as imaged on each CT slice. Next, to accurately determine the precise orientation of the millirod in the CT volume, we computed a best-fit line in three dimensions using the least squares algorithm. To determine HU values from the images, we used trilinear interpolation to obtain the signal intensity at points along concentric circles perpendicular to the 3D best-fit line and centered at the points where the fit line passed through the slices from the CT image. Thus, for each implant there was a set of concentric circles for each CT slice in which the millirod was visible, as shown in Figure 2.

Circumferentially averaged radial profiles.—To evaluate drug transport from the implant into surrounding tissue, points in the 3D image space were circumferentially averaged to yield a single 1-dimensional radial profile for each implant. Circumferential samples were obtained with an angular interval of 5° and a radial interval of one half of the in-plane pixel width (0.147 mm). Sampled points were binned by radial distance and averaged. The measurements were then compared between slices with established differences in release properties along the length of the implant. Because chemical validation of the drug release allowed no differentiation in concentrations along the length of the implant, the CT profiles were further averaged along the z-axis to yield one average profile of

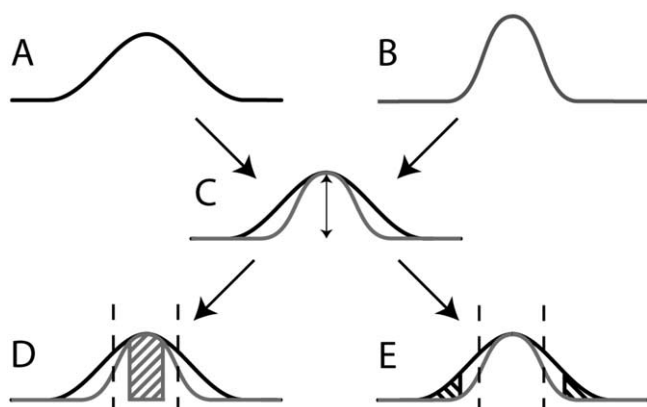


Figure 3. Schematic of algorithm used to determine carboplatin concentrations. After obtaining an experimental profile (a), the background profile generated by a rod in gelatin at time = 0 (b) was scaled to the height of the experimental profile (c). After scaling, the concentration value within the implant was determined by averaging the scaled values within 0.4 mm of the implant center (hashed region, d). The value in tissue was determined by subtracting the difference between the two profiles (hashed region, e). The dashed lines (d and e) show approximately where the implant/tissue interface would be located.

drug concentration as a function of distance from the center of the implant. This facilitated direct comparison of the CT and chemical analysis data.

Accounting for blurring of the millirod by the CT imaging system.—Because blurring of the bright signal from drug within the millirod body into the surrounding tissue may have bearing on the determination of drug concentration, we performed a control study in which a carboplatin implant was implanted into a gelatin phantom and imaged immediately after the implantation. This control determined the rod profile at $t = 0$, and the measured, circumferentially averaged profile was designated as the background profile because of a drug-containing rod in drug-free surrounding tissue. For each subsequent experimental profile, this profile was linearly scaled to the peak signal of the millirod as averaged over the innermost half of the implant (radius, <0.4 mm). The background could then be removed from subsequent measurements to obtain the drug in the tissue. Figure 3 illustrates this process.

Calculating carboplatin contained within the implant body.—To determine the average carboplatin concentration inside the millirod body, we determined the HU values of the background rod profile that had been scaled to the experimental profile. Again, those points nearest the edge of the implant (0.4–0.8 mm from the

rod center) were excluded to minimize the effects of drug inhomogeneity within the implant. To account for X-ray attenuation from the polymer component of the rod, the HU value for a PLGA polymer implant without drug was subtracted from each HU value within the drug-containing implants. The resulting difference was converted to carboplatin concentration using the in vitro rod conversion value determined as described above. Volume integration of these spatially varying concentrations for each profile allowed calculation of the drug mass present in each slice of the implant, which could then be divided by the volume to yield an average drug concentration. A mean concentration of carboplatin for the entire rod was determined by further averaging the carboplatin concentrations along the length of the device.

Calculating carboplatin concentrations within the surrounding tissue.—Carboplatin concentrations outside of the implant were determined by a similar method. First, we subtracted the background image of the rod that had been linearly scaled to the experimental profile. These HU values were then converted to carboplatin concentration by subtracting a background corresponding to either healthy or ablated liver tissue and using the in vitro conversion value determined in the gelatin phantom.

Statistical Analysis

For each experimental group, the mean drug concentration and standard deviation were calculated, and statistical comparisons were carried out with an unpaired, two-tailed Student's *t*-test. The data is reported as the mean \pm standard deviation and associated *P* values at a 95% confidence interval are included where applicable.

Correlation of CT Data With Chemical Analysis

Data obtained from the CT images was correlated with atomic absorption spectrometry (AAS) analysis of the retrieved tissue and implants as previously reported (12). To further validate the accuracy of the CT method, we calculated the average drug concentration in a tissue pillbox 0.8–4 mm from the implant/tissue interface for both the CT and AAS data. Then, treating the AAS data as a standard, the percent error (based on full data scale) was calculated. In addition, the deviation of the mean CT data from the standard was calculated to reflect the actual differences in the measurement techniques.

RESULTS

Conversion of HU to Drug Concentration

In the gelatin gels representing liver tissue only, the slope was calculated to be 15.0 HU/(mg/mL), corresponding to a sensitivity of 66.7 ($\mu\text{g}/\text{mL}$)/HU. In the millirod body, the slope was calculated to be 4.0 HU/(mg/mL), corresponding to a sensitivity of 250 ($\mu\text{g}/\text{mL}$)/HU. The minimum concentration of drug that could be measured, or detection limit, is a commonly used method for expressing the ability of a technique to detect small quantities of a substance and was estimated according to US Food and Drug Administration pharmaceutical industry guidelines (Guidance for Industry, ICH 1996) (13) using the equation $3.3 (\sigma_{\text{HU}})/\text{slope}$, where σ_{HU} = background noise (± 2 HU in our case) and the slope = HU/(mg/mL) as described above. This corresponds with a detection limit of 0.44 mg/mL in liver tissue and 1.63 mg/mL in the implant.

Carboplatin Release from the Biodegradable Polymer Implants

The release profiles of carboplatin from the millirods can be accurately quantified through examination of the implant (Figs 4, 5). Figure 4 shows the change in drug amount in the implant with time as calculated from CT image and atomic absorption analysis of the same implants (as previously reported).¹² In the ablated liver (Fig 4A), the release of drug from the polymer matrix corresponds to that in the normal liver (Fig 4B). Both environments show a rapid decrease in implant carboplatin content from 6–48 hours (from 3.3 to 1.4 mg in normal tissue and from 2.9 to 1.6 mg in ablated tissue), and while the release rate appears slower in ablated tissue from 48 to 144 hours, this difference is not statistically significant.

The dependence of drug diffusion with time on the location within the implant body is shown in Figure 5. As expected, the drug diffusion is fastest from the ends of the millirod, where the surface area is most exposed. In the central region of the implant, in turn, the release is the slowest with the minimum surface to volume ratio. This trend is consistent in the normal and ablated livers, and the differences between the outermost and center sampling points are significant ($P < .05$) at all time points. Another point of interest is the lack of drug release between 96–144 hours in the ablated system, which is not seen in the normal liver tissue. Although these findings are not surprising, the fact that they were deter-

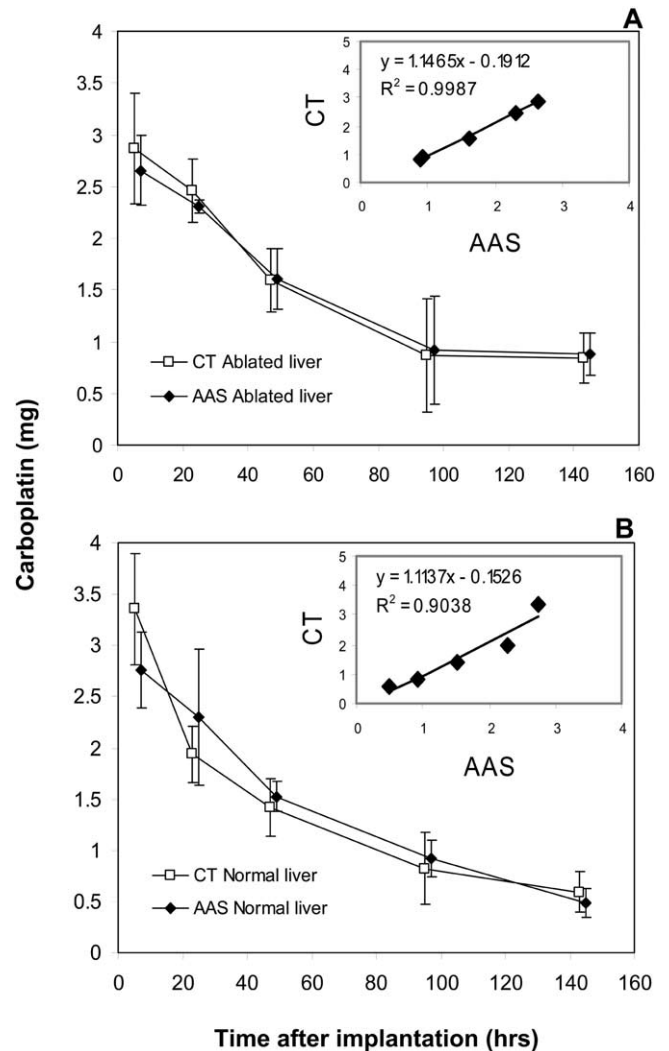


Figure 4. Release of carboplatin from polymer implants in ablated (a) and normal (b) livers. The release was monitored with CT noninvasively and was correlated with atomic absorption measurements of retrieved implants. Superior correlation of data validates the CT method in this application. Data represents mean \pm SD ($n=3$). Curves were intentionally offset for clarity of presentation.

mined noninvasively in a physiologic setting is encouraging and can lead to other potential applications of this technique.

Tissue Penetration and Distribution of Carboplatin in Normal and Ablated Tissue

Figure 6 shows distribution of carboplatin in the surrounding liver. Between 0.8–1.6 mm from the center of the rod, the abrupt implant/tissue interface causes an artifact, thus we focused our analysis on the data only outside this region. Similarly, we do not show drug concen-

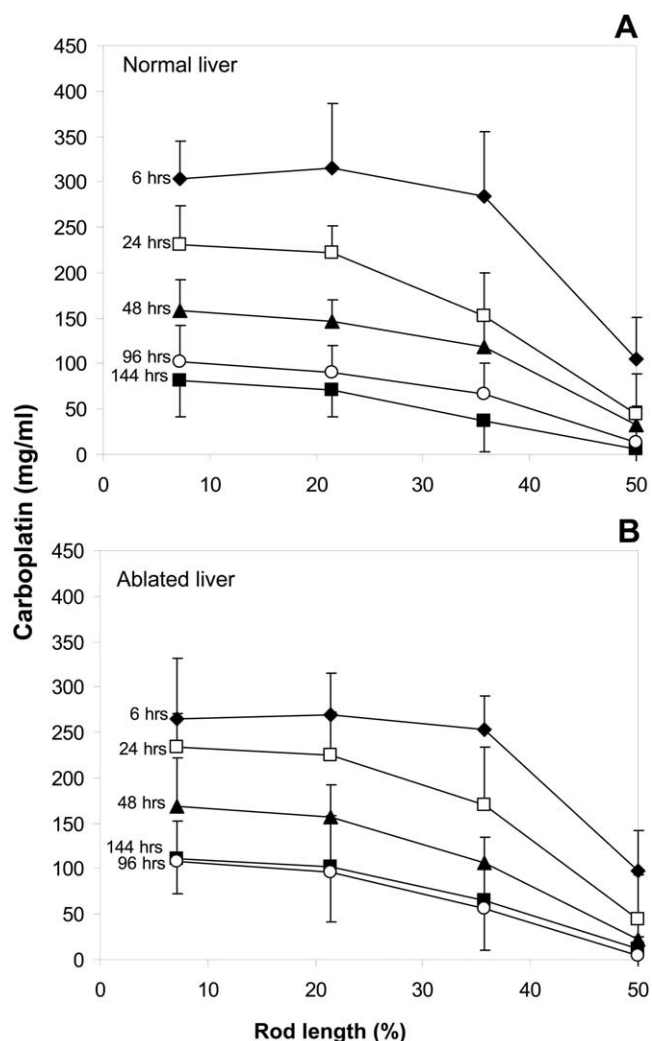


Figure 5. Release of carboplatin along the length of implanted rod. CT was utilized to examine the differences in drug release along the length of each implant correlated with implantation time. As expected, the release is faster along the ends and slowest in the middle of the rods. Data represents mean \pm SE. Portions of error bars were omitted for clarity.

trations for distances greater than 4 mm from the implant boundary for two reasons: variation in the distance of the ablation boundary from the implant in ablated liver and undetectably low concentrations of drug present at distances greater than 4 mm. The results show the distribution of drug as it diffuses into the surrounding tissue and is cleared by the local vasculature. The tissue penetration is more extensive in the ablated tissue, with the drug concentration peaking at 48 hours. At the first sampling point (1.6 mm from the implant center) carboplatin concentration is significantly higher in ablated tissue at 48 ($P = .002$), 96 ($P = .014$), and 144 ($P = .002$) hours. The

drug concentration in ablated tissue reaches 4.7, 3.3, and 3.6 mg/mL at 48, 96, and 144 hours, respectively. In comparison, the concentration in normal liver at 1.6 mm reaches 0.7, 0.5, and 0.9 mg/mL at 48, 96, and 144 hours, respectively. At 2.8 mm, the difference is significant at 48 hours ($P = .042$), and just below the level of significance at 96 ($P = .089$) and 144 ($P = .111$) hours. This is most likely due to the high inter-animal variability. At 4 mm, we speculate that the drug is beyond the ablated liver boundary and is washed away by normal liver perfusion, and there are no differences between drug concentration in ablated and normal liver.

Carboplatin penetrates into the ablated tissue to a much greater extent and consequently the maximum penetration distance is longer in ablated liver than normal liver. We defined the maximum penetration distance as the distance from the implant/tissue interface to which the drug level is above the lower detection limit of CT (0.44 mg/mL). The drug reaches 3.1 mm in ablated liver compared with 2.3 mm in normal liver at 48 hours ($P = .027$). After 144 hours, the drug is still detected at 3.1 mm in ablated liver but drops to 0.8 mm in normal liver, meaning that no drug could be detected outside of the implant at this time ($P = .007$). At 24 and 96 hours, the differences are not significant.

Seen in Figure 6F is a representative plot of the inter-versus intra-animal variability for one experimental group (ablated liver, 24 hours). The figure clearly shows the high variability between animals and stresses the potential value of using the noninvasive CT method for screening the drug release in a single animal over time.

Correlation of CT Data With Chemical Analysis

The data from this study were compared with AAS analysis of carboplatin content in both the implants removed immediately after the CT scan and the liver tissue as reported previously (12). It is apparent that the CT data accurately predicts the kinetics in this system despite the small size of the implant, and this is true in both ablated (Fig. 4A) and normal (Fig. 4B) livers. The correlation of the CT and AAS data within the implant body is emphasized in the Figure 4 inserts. The R^2 values and slopes of the best fit lines obtained from the linear correlation plots were 0.999 (slope = 1.15) and 0.904 (slope = 1.11) for ablated and normal livers, respectively. The slope, which should ideally be equal to 1, is slightly higher because cylindrical volume used to make this measurement includes only the centermost region of the implant.

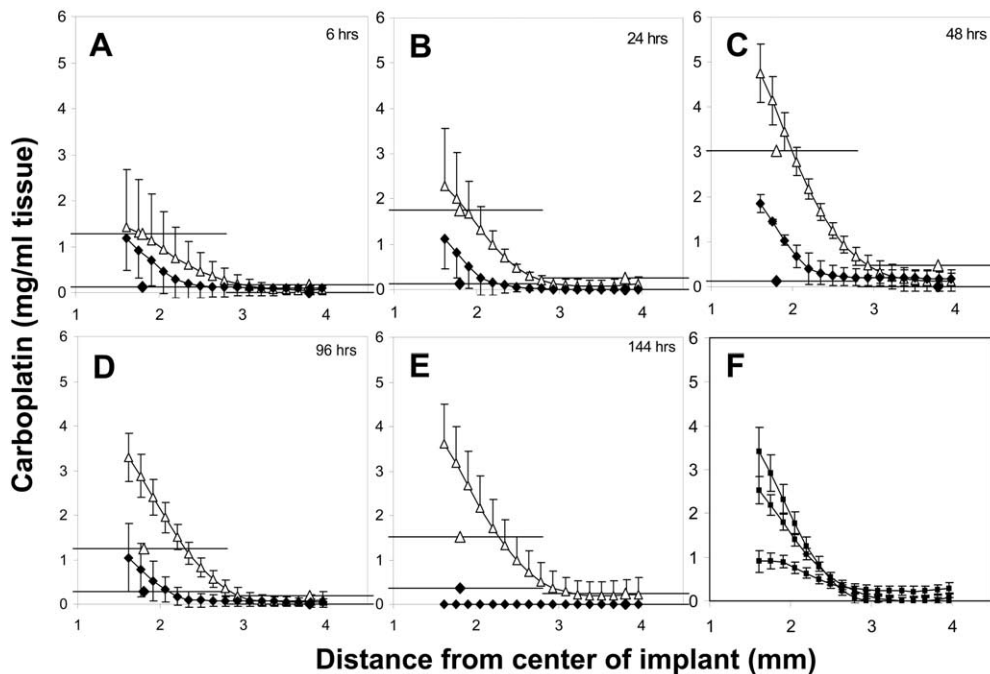


Figure 6a-e. Carboplatin distribution in normal (◆) and ablated (△) liver tissue measured by CT (line plot) and atomic absorption spectroscopy (horizontal bars). Values reflect mean ± SD between animals. Horizontal bars in the AAS data represent the average drug concentration determined over a tissue sample the width of the bar. **(f).** Carboplatin distribution at 24 hrs in 3 separate animals demonstrating the intra- and inter-animal variability. This plot corresponds to the mean data shown in Figure 5B.

A similar correlation was carried out for the tissue distribution measurements. Figure 6 shows the comparison of CT and AAS data when examining the carboplatin concentration within tissue, where the CT data was obtained from the profile analysis of the tissue volume. The CT data overestimates the drug content determined by the AAS data predominantly between 1–2 mm and underestimates it as the distance from the implant increased. At distances further away from the implant, the CT profile data describes the retention and penetration of the carboplatin as more extensive in the ablated liver, but it is not accurate at the low drug concentrations detected by AAS (quantification limit 25 ppb). This is most evident when looking at the normal liver release, where most of the concentration measurements at points exceeding 2 mm from the implant boundary become negative because of image noise and background subtraction. It should be noted that the negative concentration values were set equal to zero for display purposes.

Results shown in Figure 7 describe the quantitative change in drug concentration as a function of time for a tissue volume from 0.8–3.2 mm from the implant boundary. In the ablated liver, the percent error was below 21%

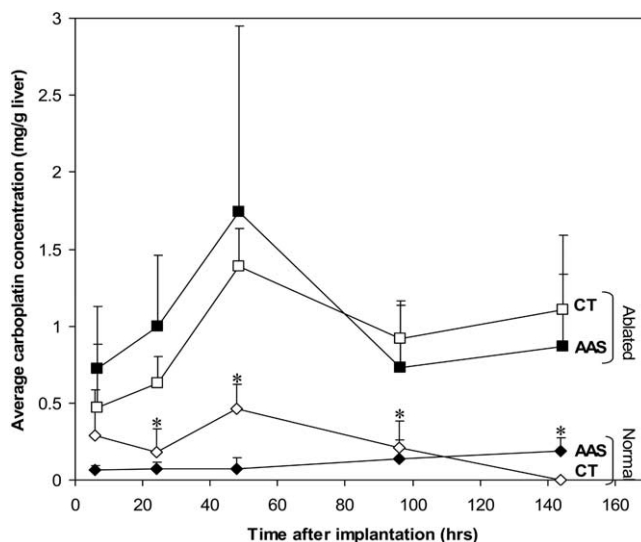


Figure 7. Change with time of average carboplatin concentration in normal and ablated liver tissue volumes 0.8–3.2 mm from the implant-tissue interface as determined by CT (◇, □) and AAS (■, ◆). Data represents mean ± SD. *p<0.05 significant difference determined between average carboplatin concentration in normal and ablated livers based on CT data.

but exceeded 38% in the normal liver for all six sampling points. The deviation of measurement ranged from 0.19–0.37 mg/g in ablated liver and 0.07–0.40 mg/g in normal liver. Also shown in Figure 7 is the significant difference between the drug concentrations in normal and ablated tissue volumes. The carboplatin concentration remains above 0.6 mg/mL after 24 hours in the ablated tissue (a consistent 3-fold increase over normal) and this difference is significant ($P < .05$) at 24–144 hours. In the ablated liver, the concentration of carboplatin is sufficiently high and can be detected by CT with fair correlation to the actual concentration (from AAS). However, when the drug concentration decreases, the accuracy of the CT detection diminishes. The quantum noise combined with background subtraction lead to a negative concentration value which should be regarded as zero. This is again the effect of insufficient sensitivity in the CT imaging.

DISCUSSION

We have shown the successful use of X-ray CT, a common diagnostic imaging technique, for a functional application – examining the kinetics of local drug delivery in vivo. High spatial and temporal resolution, and relatively high sensitivity combined with low image noise (roughly ± 2 HU) of CT offer an unprecedented opportunity in noninvasive pharmacokinetic imaging. Although the detection limit of the CT method is inferior to methods such as positron emission tomography (10^{-12} versus 10^{-4} mol/L for CT) (14), with appropriate image analysis techniques, CT has the resolution to provide both qualitative and quantitative information about the pharmacokinetic behavior of appropriately chosen chemotherapeutic agents.

This work extends beyond that reported previously and highlights the capabilities of CT in noninvasively evaluating the release and tissue penetration of a drug in an animal model. Previous studies in our group have established this functional application of CT in a gelatin phantom and animal model (10,15,16). We have shown that CT can accurately quantify the local release kinetics of a model drug, iohexol, from a device implanted in an animal by correlation to chemical analysis of the same data (10,15). In addition, we have shown the feasibility of this technique combined with image analysis in quantifying the drug distribution within liver tissue (16). Here, we report on a specific application of the CT technique in examin-

ing the release kinetics of an anticancer drug, carboplatin, from a polymer implant into rat livers following radiofrequency ablation. Using a more robust, volume-based image analysis regimen than previously reported (16), we developed a simple and effective method of calculating clinically relevant pharmacokinetic data in our animal model that cannot be easily obtained by any other means.

Characterization of Local Carboplatin Release in Normal and Ablated Liver Tissue

The drug delivery implant used in this study consists of a biodegradable polymer matrix entrapping a chemotherapeutic agent, carboplatin. Our previous studies have shown the feasibility of modulating the drug release kinetics from these implants for local drug therapy (8,17). Because it contains platinum, the drug can be visualized with X-ray imaging and quantified through image analysis based on the linear relationship between X-ray attenuation and concentration of Pt atoms in a sample. This data, in turn, can provide valuable insight regarding the drug transport processes in an undisturbed physiologic system. Subsequently, this information can be used to better understand the delivery of a drug to a lesion created by radiofrequency ablation and improve on one of the drawbacks of this therapy – incomplete elimination of cancerous cells at the peripheral tumor boundary (18,19). Because the ablated tissue differs drastically from healthy, highly vascularized liver tissue, traditional pharmacokinetic models cannot predict the drug movement in this system. Noninvasive imaging can aid in the understanding of this system and in future rational design of a device with maximum therapeutic efficacy at the site of action.

It is well documented that the greatest effect of radiofrequency ablation on the tissue is cell necrosis and destruction of vasculature, which are thought to be responsible for the increased retention of drug in the ablated lesion (6–10,20,21). Because a minimal amount of drug is lost by perfusion, this suggests that the dominant drug transport in the system may be diffusion, which is a drastically slower process. Thus, the retention of the drug is enhanced and clearance is lowered in the ablated region. This is also clear by the increased measurable penetration distance, a fact somewhat evident from the CT data and clearly defined by the chemical analysis of tissue drug levels. The latter approximates the maximum penetration to be close to the approximate ablation boundary (measured at 5 mm). In contrast, the normal liver is highly

perfused, which allows quick and uninterrupted dissolution of the drug from the polymer matrix and its clearance from the tissue.

Processing of CT Images to Obtain Accurate Pharmacokinetic Data

In the present application of CT, image processing is critical for acquisition of clinically relevant pharmacokinetic data. Image sampling and background subtraction as well as accurate conversion value measurement are essential for accurate system description. The fitting of a line to the center of the cylindrical implant allows sampling of data at an orientation exactly perpendicular to the long axis of the millirod, optimizing the circumferential averaging process and allowing simple region of interest analysis. We have chosen to circumferentially average the signal from a control image set, and then linearly scale and subtract this profile from the experimental profiles to determine the carboplatin concentrations both within the implants and in the tissue surrounding them. Although this set of experiments included background subtraction of a drug-free rod implanted in gelatin, the addition of an *in vivo* background image of a rod containing no drug taken at each time point may improve upon the current correlation between CT measurements of drug concentration and chemical validation studies.

Data correlation indicates that the CT method overestimates the drug concentrations in tissue. This phenomenon is most likely a result of two factors: (1.) the inherent blur artifact associated with small bright objects (eg, millirods) placed in a larger and less-attenuating matrix (eg, liver tissue), and (2.) the beam hardening artifact resulting from the high contrast difference between the millirod and the tissue. Both of the artifacts are clearly visible in the CT images, and although found in the normal liver, the effects are more notable in the ablated tissue (which has gray levels approximately 30 HU lower than the normal liver). It is also evident that the greatest overestimation occurs at distances closest to the implant boundary and lessens with increasing radius as well as with time, as can be noted on the 6 hour versus 96 hour profiles. The less than optimal correlation can also be attributed in part to the difference in spatial resolution of the two methods. AAS sampling occurred at a frequency of 2 mm compared with the sub-mm sampling of the CT.

Potential Improvements and Future Work

While we have attempted to address all aspects of this multifaceted process, further investigation is warranted,

especially in the radial profile analysis. Although we have significantly improved on the previous analysis, many potential improvements can still be undertaken. For example, blurring, which most likely is responsible for the overestimation of drug concentration adjacent to the implant/tissue boundary, can be diminished by changing the reconstruction filter to obtain a more accurate drug release profile.

It is clear that the detection limit of the current CT technique (which is highly dependent on image noise) is too low to adequately describe the minute drug levels present in the tissue. The clear benefits of the CT monitoring lie instead in the analysis of release from the implants and in the relative comparisons of drug release and distribution in different systems. It can already be seen that the technique does detect a difference between the normal and ablated liver distribution (as seen in the maximum penetration distance analysis). However, the absolute, accurate quantification of drug concentrations is not feasible at this time. These issues can potentially be addressed by maximizing the signal-to-noise ratio by increasing the number of X-ray photons passing through the animal (mA), lengthening the rotation time or increasing the slice thickness. All of these require further investigation to optimize and expand the applications of this method. Nonetheless, this noninvasive imaging method has been thus far exceedingly productive in collecting data on the unperturbed physiologic processes affecting local drug therapy. Although the data correlates well with chemical analysis of the drug levels in implants, the limited X-ray absorption of carboplatin hampers accurate measurement of low drug levels in tissue. The acquired data is useful in predicting trends in the system but lacks the sensitivity necessary to obtain quantitative spatially varying pharmacokinetic data.

CONCLUSION

X-ray CT was used in the evaluation of local pharmacokinetics of a drug delivered directly to the site of action by means of a polymer implant. The release rate and tissue distribution of carboplatin were determined through a robust, image volume analysis regimen in a rat model over 144 hours. In addition, the data were used to determine the distribution of the drug within the body of the polymer matrix and its changes with time. Results show that ablation of liver tissue led to slower drug release from the polymer implants and larger tissue penetration

compared with normal livers. The significant change of physiologic environment caused by ablation and its subsequent effect on drug pharmacokinetics must be considered when designing a drug delivery device to be used in conjunction with radiofrequency ablation.

Direct validation of the technique was made possible through correlation of CT data with chemical analysis of removed implants and surrounding tissue. The correlation showed a notable similarity between the CT image prediction and actual drug concentration within the implant. Adequate correlation was also seen in the tissue distribution, but a less than optimal sensitivity and blurring artifact may account for errors in the profile correlation. Overall, the method provides a simple and convincing approach for monitoring in vivo drug release in agents able to attenuate X-rays, but additional work is required for the technique to be the sole assessment of tissue distribution (by radial profiles) at low drug concentrations. Nonetheless, evidence is compelling that this method is quite capable in evaluating the release of an agent from a small drug delivery device and noninvasively acquiring data unavailable by any other means. The results of this work could potentially reduce inter-animal variability common in in vivo evaluations of local therapies and could significantly reduce the number of animals required to carry out these studies.

ACKNOWLEDGMENT

The authors thank all those associated with this extensive project, especially Leslie Ciancibello and Dr. Uri Shreter for their CT expertise, and Kim Shreter for her help with the CT image analysis.

REFERENCES

- Port RE, Wolf W. Noninvasive methods to study drug distribution. *Invest New Drugs* 2003; 21:157-168.
- Singh M, Waluch V. Physics and instrumentation for imaging in-vivo drug distribution. *Adv Drug Deliv Rev* 2000; 41:7-20.
- Bhatnagar A, Hustinx R, Alavi A. Nuclear imaging methods for non-invasive drug monitoring. *Adv Drug Deliv Rev* 2000; 41:41-54.
- Taylor JS, Reddick WE. Evolution from empirical dynamic contrast-enhanced magnetic resonance imaging to pharmacokinetic MRI. *Adv Drug Deliv Rev* 2000; 41:91-110.
- Nguyen TT, Pannu YS, Sung C, et al. Convective distribution of macromolecules in the primate brain demonstrated using computerized tomography and magnetic resonance imaging. *J Neurosurg* 2003; 98:584-590.
- Ahmed M, Monsky WE, Gimm G, et al. Radiofrequency thermal ablation sharply increases intratumoral liposomal doxorubicin accumulation and tumor coagulation. *Cancer Res* 2003; 63:6327-6333.
- Monsky WL, Kruskal JB, Lukyanov AN, et al. Radio-frequency ablation increases intratumoral liposomal doxorubicin accumulation in a rat breast tumor model. *Radiology* 2002; 224:823-829.
- Qian F, Stowe N, Saidel GM, et al. Comparison of doxorubicin concentration profiles in radiofrequency-ablated rat livers from sustained- and dual-release PLGA millirods. *Pharm Res* 2004; 21:394-399.
- Gao J, Qian F, Szymanski-Exner A, et al. In vivo drug distribution dynamics in thermoablated and normal rabbit livers from biodegradable polymers. *J Biomed Mater Res* 2002; 62:308-314.
- Szymanski-Exner A, Stowe NT, Lazebnik RS, et al. Noninvasive monitoring of local drug release in a rabbit radiofrequency (RF) ablation model using x-ray computed tomography. *J Control Release* 2002; 83:415-425.
- Qian F, Szymanski A, Gao J. Fabrication and characterization of controlled release poly(D,L-lactide-co-glycolide) millirods. *J Biomed Mater Res* 2001; 55:512-522.
- Szymanski-Exner A, Gallacher A, Stowe NT, et al. Local carboplatin delivery and tissue distribution in livers after radiofrequency ablation. *J Biomed Mater Res* 2003; 67A:510-516.
- Center for Biologics Evaluation and Research. Food and Drug Administration Web site. Available at: <http://www.fda.gov/cber/guidelines.htm>.
- Fischman AJ, Alpert NM, Rubin RH. Pharmacokinetic imaging: A noninvasive method for determining drug distribution and action. *Clin Pharmacokinet* 2002; 41:581-602.
- Szymanski-Exner A, Stowe NT, Salem K, et al. Noninvasive monitoring of local drug release using x-ray computed tomography: Optimization and in vitro/in vivo validation. *J Pharm Sci* 2003; 92:289-296.
- Salem KA, Szymanski-Exner A, Lazebnik RS, et al. X-ray computed tomography methods for in vivo evaluation of local drug release systems. *IEEE Trans Med Imaging* 2002; 21:1310-1316.
- Qian F, Saidel GM, Sutton DM, et al. Combined modeling and experimental approach for the development of dual-release polymer millirods. *J Control Release* 2002; 83:427-435.
- Goldberg SN, Gazelle GS. Radiofrequency tissue ablation: Physical principles and techniques for increasing coagulation necrosis. *Hepato-gastroenterology* 2001; 48:359-367.
- Goldberg SN. Radiofrequency tumor ablation: principles and techniques. *Eur J Ultrasound* 2001; 13:129-147.
- Lewin JS, Connell CF, Duerk JL, et al. Interactive MRI-guided radiofrequency interstitial thermal ablation of abdominal tumors: Clinical trial for evaluation of safety and feasibility. *J Magn Reson Imaging* 1998; 8:40-47.
- Goldberg SN, Gazelle GS, Compton CC, et al. Treatment of intrahepatic malignancy with radiofrequency ablation: Radiologic-pathologic correlation. *Cancer* 2000; 88:2452-2463.